Tellus (1997), 49A, 577–594
Printed in UK – all rights reserved

TELLUS
ISSN 0280–6495

Binary interactions between polar lows

By IAN A. RENFREW*, G. W. K. MOORE and AASHISH A. CLERK**, *Department of Physics, University of Toronto, 60 St. George Street, Toronto, Ontario M5S 1A7, Canada*

(Manuscript received 2 December 1996; in final form 8 July 1997)

ABSTRACT

In this study, the movement of polar lows is addressed from a novel and perspicuous viewpoint. The usual assumption has been that these mesoscale systems are, to a first approximation, advected by the larger scale flow in which they are embedded. However, when there are two or more polar lows in the same vicinity, binary interactions between pairs of polar lows can cause a cyclonic co-rotation of the pair. In geographic coordinates these interactions can appear as unusual loops, twists and turns in the low tracks, due to the interplay between the cyclonic co-rotation and the translation of the binary pair by the ambient flow. However when the tracks are replotted in centroid relative coordinates, a mutual rotation is unmistakable. Satellite imagery from several case studies has been examined to accurately determine the polar low tracks, and thus the co-rotations. Using surface wind observations, a theoretical rotation rate can be estimated, based on barotropic vortex dynamics. There is a good correspondence between the observed and calculated rotation rates. Recognizing the existence of binary interactions between polar lows emphasises the connection between polar lows and tropical cyclones, where binary interactions have been described in several studies. Indeed, in the cases studied here, binary interactions are strongest during the secondary (convective) stage of polar low development where the lows are somewhat analogous to arctic hurricanes.

1. Introduction

The movement of polar lows is not well understood; yet it is of vital importance for operational forecasting that polar low tracks are accurately predicted. The lack of attention is due, in part, to two factors: the chronic shortage of accurate observations at high latitudes, and the tacit assumption that these mesoscale cyclones are, to a first approximation, advected by the larger scale flow (Businger and Reed, 1989). The lack of ground and upper air observations is an immutable problem at high latitudes, and as a consequence in this study satellite imagery is used as the primary source of information. The second point, that polar lows are simply advected (or steered) by the surrounding synoptic scale systems appears a reasonable first approximation for isolated polar lows. However it is not the case when several polar lows co-exist in the same area. Instead, as this study demonstrates, interactions between pairs of polar lows cause unusual twists and turns in their tracks, as the lows influence each other's movement. Such binary interactions between adjacent atmospheric vortices have been observed in the tropics (e.g., Haurwitz, 1951; Brand, 1970; Dong and Neumann, 1983; Lander and Holland, 1993), and to a less ubiquitous extent at mid-latitudes (Ziv and Alpert, 1995). However they have not been previously examined at high latitudes.

Binary interactions between vortices were first noted in the laboratory experiments of Fujiwhara (1923, 1931). Fujiwhara demonstrated that two cyclonic vortices rotate around each other in a

* Corresponding author.
email — ian@atmosp.physics.utoronto.ca
** Present affiliation: Department of Physics, Cornell University, Ithaca, New York, 14853–2501, USA.

cyclonic sense, and undergo a mutual attraction, leading to an eventual merger. The rotational effect can be reproduced by two positive point vortices (or two constant vorticity patches) in a stationary barotropic fluid. In this scenario, the cyclonic flow field induced by each positive vortex advects the other vortex in a cyclonic sense, so they will co-rotate around their centroid (or centre-of-mass). If the vortices are of equal magnitude then their centroid is the midpoint of the line connecting their centres. Further laboratory experiments and a number of numerical modelling studies have also demonstrated this basic result for barotropic vortices (see Hopfinger and Van Heijst, 1993 for references).

In a meteorological context, Haurwitz (1951), Brand (1970) and Dong and Neumann (1983) examined binary interactions between tropical cyclones. The Haurwitz (1951) study suffered from a lack of reliable data and many discrepancies with the Fujiwhara model were found, for example in the estimates of the rotation rates of the tropical cyclones. Brand (1970) found a co-rotation that was strongly dependent on the separation distance of the tropical cyclones, although this co-rotation could be overshadowed by the environmental flow in which the cyclones were embedded. Dong and Neumann (1983) discussed this in more detail, examining the role of the Intertropical Convergence Zone in modifying rotation rates. Motivated by the importance of this problem for tropical cyclone track prediction, a hierarchial series of papers by Holland and co-workers has recently been published. Lander and Holland (1993) presented a detailed observational study of binary interaction and vortex merger for tropical cyclones. In Ritchie and Holland (1993) a vortex patch model was used to examine the co-rotation of equal, and unequal, vortices in a barotropic fluid. In Holland and Dietachmayer (1993) a more complex continuous barotropic vortex model was developed, and in Wang and Holland (1995) a baroclinic model gave a more detailed picture of a variety of vortex interactions. The interaction paradigm which arises from these studies can be summarised as consisting of the following 3 distinct stages: (i) *approach and capture*: the vortices somehow move towards one another until mutual advection by the cyclonic flow fields begins; (ii) *mutual orbit*: the vortices co-rotate around their centroid; (iii) *merger or escape*: the cyclones merge if separated by less than some critical distance, *or* escape from the mutual orbit. The merger occurs by a distortion of the vortices' symmetry which leads to a shearing of each vortex into the other. If the cyclones do not come close enough to merge, a rapid escape ensues due to nonlinear interactions between the rotating cyclones and their environment (e.g., a subtropical ridge or the planetary vorticity gradient). Ritchie and Holland (1993) obtained a critical separation distance, below which merger occurs, of $3.2R$, where R is the radius (from the vortex centre) of the maximum azimuthal wind. Interactions between tropical cyclones and smaller systems embedded within the tropical cyclone circulation are examined in a companion paper (Holland and Lander, 1993), which investigates the variety of meanders in tropical cyclone tracks.

The key point for atmospheric vortex movement and forecasting, is that such binary interactions may *not* be obvious in a geographic coordinate frame. If there is an ambient or environmental flow, then the combination of the co-rotation and the ambient flow translation results in complicated vortex tracks, with a variety of twists and turns (Rasmussen, 1985a; Ritchie and Holland, 1993). However when viewed in a "centroid relative" coordinate frame the translation of the centroid of the binary system is removed, and the co-rotation of the vortex pair becomes clear.

In the tropics the ambient (or environmental) flow in which tropical cyclones are embedded will be relatively small compared to the flow fields associated with the cyclones themselves — in the vicinity of the systems at least. (Note the reader is referred to Gill (1982), and James (1994) for evidence on the general nature of the ambient or "mean" flow at different latitudes). So the approximation of a stationary (or near stationary) barotropic atmosphere is reasonable. In contrast, at mid-latitudes the zonally averaged mean flow is dominated by a strong westerly jet. Baroclinic eddies grow as a wavetrain of instabilities, or finite amplitude waves, on this zonal jet and are of comparable scale to the jet itself. Thus mid-latitude binary interactions are likely be overshadowed by other dynamical processes, such as differential advection by the spatially varying mean flow, or propagation of the wave instabilities. As a consequence, the idealisation of a near stationary and barotropic atmosphere is not appropriate at mid-

latitudes. Ziv and Alpert (1995) employed a statistical analyses of 7 years of initialised analyses to investigate the co-rotation of mid-latitude cyclones in the Mediterranean region. They found a clear cyclonic co-rotation only when the separation distance of the cyclone pair was relatively small. Indicating co-rotation was only a feature for mesoscale lows (e.g., Mediterranean lows) and not a factor for the more typical synoptic scale lows found at mid-latitudes. The composite rotation rates they found were small (a maximum of 0.6° per hour) and could be partly explained by a cyclonic shear of the mean flow at mid-latitudes.

At high latitudes, although the atmosphere is far from stationary and barotropic, a case can be made that binary interactions play an important role in cyclone movement. The zonal jet is less dominant at higher latitudes, as it is present only periodically, depending upon large scale weather regimes (Vautard, 1990). Furthermore, polar lows are relatively small in scale but intense in circulation, with a significant contribution to development coming from convective processes (Businger and Reed, 1989; Rasmussen, 1989). The small scale implies that they can exist close to one another, developing under similar convectively unstable conditions, and if sufficiently intensive, then within each other's induced flow field. Due to their proximity, both lows in a pair would undergo similar influences from the ambient flow. In other words, the scale of the binary system is less than the scale of major ambient flow variations, so the system would be translated as a whole by the synoptic scale flow. In addition, the convective intensification process common to both tropical cyclones and polar lows allows the growth and maintenance of these systems away from areas of large horizontal shear (Craig and Cho, 1992). This relative isolation would allow binary interactions to dominate system movement, at the expense of the dynamical processes associated with such horizontal shears; again a reason for binary interactions to occur preferentially at low latitudes and high latitudes, rather than mid-latitudes.

This investigation employs several case studies to examine binary interactions between polar lows. In section 2 a simple co-rotation theory is detailed for a barotropic fluid. In sections 3 and 4 two polar low episodes are examined. Satellite data are used to determine the vortex tracks, and where available surface wind data are used to quantitatively compare the observed interactions with the simple theoretical model. Conclusions are presented in section 5.

2. Theoretical summary

In a barotropic fluid at rest, each vortex in a binary pair can be idealised as a Rankine vortex, ie. a vortex with an inner core in solid body rotation, with angular velocity Ω, and an outer circulation where the azimuthal velocity scales as $1/r$ (Haurwitz, 1951). The velocity profile is defined as:

$$V=\begin{cases} \Omega r = V_m \dfrac{r}{R_m}, & r \leqslant R_m \\ \Omega \dfrac{R_m^2}{r} = V_m \dfrac{R_m}{r}, & r > R_m, \end{cases} \tag{1}$$

where r is radial distance and R_m is the radius of maximum wind V_m. Each Rankine vortex consists of a core patch of constant relative vorticity ($\xi = 2\Omega$), in a zero vorticity environment. This appears a reasonable first approximation for polar lows: compare for example the wind profiles in Fig. 11 reproduced from Rasmussen et al. (1992, hereafter RPPT) and the discussion in Rasmussen (1989)†.

The rotation of the two vortices is due solely to mutual advection, hence the rotation rate (ω) for the line connecting the vortex pair is

$$\omega = \frac{V_{AB} + V_{BA}}{d}, \tag{2}$$

where V_{AB} is the velocity induced by vortex A at vortex B, V_{BA} is the velocity induced by B at A, and d is the distance between the vortex centres (Fig. 1). Assuming the velocity profiles in (1), and as the inner cores are small ($d > R_A + R_B$), then each vortex in the pair is advected by the others *outer* circulation. Hence this gives:

$$\omega = \frac{V_{Am}R_{Am} + V_{Bm}R_{Bm}}{d}, \tag{3}$$

The stationary point in the binary system (indi-

† Note for tropical cyclones a $1/r^{\frac{1}{2}}$ azimuthal wind profile is thought to be more appropriate (Anthes 1982) and this profile does give a better correspondence to the tropical cyclone data assessed in Brand (1970).

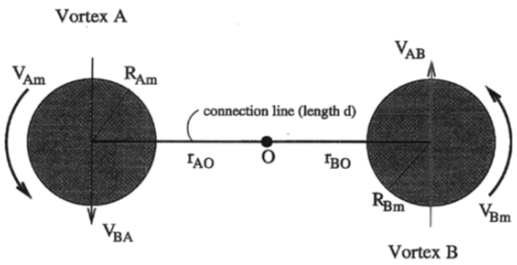

Fig. 1. Schematic of a binary vortex pair.

cated by an "O" on Fig. 1) is called the centroid of the binary system. If the distance d is divided into r_{AO} and r_{BO}, where r_{AO} is the distance from vortex A to O, and r_{BO} is the distance from vortex B to O; then by geometric arguments, to remain stationary:

$$\frac{r_{AO}}{r_{BO}}=\frac{V_{BA}}{V_{AB}}=\frac{M_B}{M_A}, \tag{4}$$

where M_A and M_B are the "masses" of vortices A and B, defined by $M=\Omega R_m^2$ (Haurwitz, 1951). The definition of the vortex masses draws an analogy between the binary vortex pair and the classic two body problem, with the centroid analogous to the centre-of-mass of the two bodies. If there is no ambient flow present, then the centroid remains fixed and the vortices rotate around it, perpendicular to their connection line (cf. Fig. 1). If an ambient flow is present, then the co-rotation will be in addition to a translation of the entire binary system by the ambient flow.

Note that the same rotation rate can be deduced for two point vortices in a stationary background flow (Batchelor, 1980; Ziv and Alpert, 1995). Ziv and Alpert also derived a rotation rate for a cyclone pair embedded within a constant background shear. As outlined earlier the background shear is assumed not to be as important for a mesoscale polar low system and so this is not accounted for in the simple theory used here. In the following sections eq. (3) is used to estimate a theoretical rotation rate ω, for comparison with the observed rotation rates.

3. The December 1982 case

An outbreak of polar lows over the Barents Sea area in December 1982 provides our first case

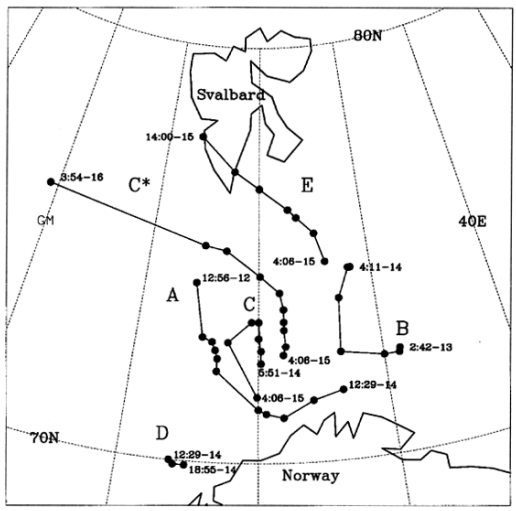

Fig. 2. Tracks of polar lows and other disturbances in the Barents Sea area over the period of 12 to 16 December 1982. Lines of latitude and longitude are every 10°. The start and end time-dates of each vortex are labelled in the format hh:mm-dd.

study. This event has been studied extensively by Rasmussen (1985a) and RPPT.‡ These two papers provide a comprehensive report on the background synoptic picture and the development of a variety of polar low disturbances that occurred during this time. Fig. 2 plots the tracks of the polar lows for the period of the 12 to 16 December 1982, as determined from satellite imagery. Note for consistency we follow the nomenclature of RPPT. Over the period, a variety of disturbances are present and as shown in Fig. 2 their movements appear quite complicated; any interactions between the disturbances are not obvious. However as we shall see, a careful examination of the co-existing polar lows results in a considerable simplification of the picture.

3.1. *Polar low motion*

The first polar low (A) was triggered by an upper level potential vorticity anomaly moving

‡ Note it came to the authors attention during the review process that an unpublished technical report (Rasmussen, 1985b) mentioned the likelihood of the Fuijwhara effect causing a co-rotation of lows A and B. However this was not pointed out in the two published studies on this polar low episode, or anywhere else in the literature.

over a low level baroclinic zone that had been generated by cold air advection off the sea ice surrounding Svalbard (see RPPT). A baroclinic instability process, following the paradigm described in Hoskins et al. (1985), results in the initial spin up of vortex A. Fig. 3 shows an infra-red satellite image of polar low A at 02:42 GMT on 13 December 1982. Around this time low A evolves from the initial baroclinic development phase into a more convective phase, as indicated by the satellite imagery which clearly shows the development of convective cells (Fig. 3). A few hours later the convective nature of low A is further indicated by the small scale of the central vortex, a rapid pressure drop, and the radiosonde soundings from a weather ship "AMI" (see RPPT). As A evolves into this second phase other disturbances become visible in the satellite imagery. Polar low B is visible as a curvature in the cloud cluster east of A in Fig. 3, and 12 h later at 12:44 GMT

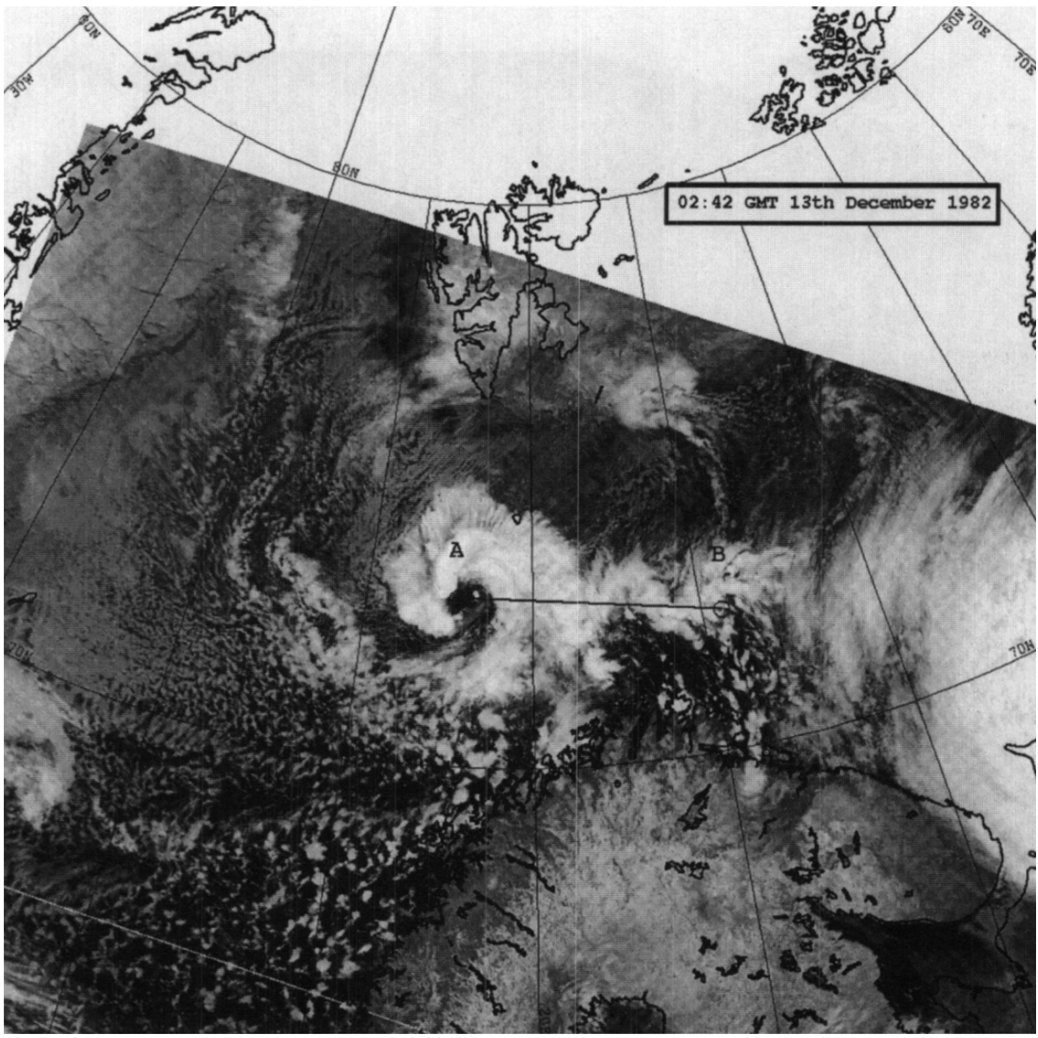

Fig. 3. AVHRR infra-red satellite image (channel 4) of the Barents Sea area at 02:42 GMT on 13 December 1982 from the NOAA-7 pass. Lines of latitude and longitude are overlaid every 10°. Polar lows A and B are marked and a connection line joins their centres. Low A is well defined by a spiral of high clouds with embedded convective cells clearly visible. Polar low B, to the east, is just forming a vortex-like cloud signature.

on 13 December 1982 (Fig. 4), both A and B are well defined as polar lows. After a further 13 h at 04:11 GMT on 14 December 1982 (Fig. 5), A and B have moved southeast and northwest respectively, and a smaller scale disturbance is also visible (vortex C on Fig. 2) between A and B. To quote RPPT "the synoptic scale low was in fact, at that time, a conglomerate of several subsynoptic/mesoscale phenomena".

The satellite derived tracks of polar lows A and B are plotted in Fig. 6a, low A tracks south, southeast then east; low B tracks west then north. Note low A is longer lived than low B. For details on deriving vortex tracks from satellite imagery, please see the Appendix. The path of the centroid of A and B, calculated as the unweighted mean (in map coordinates) is also shown. Note the mapping is a stereographic projection centred at 75°N, 20°E so is very nearly isometric in the area of interest. The centroid executes a small anticyclonic loop, indicating little translation of the binary system as a whole. When the tracks are

Fig. 4. IR satellite image at 12:44 GMT on 13 December 1982 from the NOAA-7 pass. Polar lows A and B are marked, note A has a clear central eye.

Fig. 5. IR satellite image at 04:11 GMT on 14 December 1982 from the NOAA-7 pass. Polar lows A and B are marked.

replotted in centroid relative coordinates (Fig. 6b) an interaction between A and B is clear. The lows approach each other (over the first few hours of co-existence), are captured, and then co-rotate from 12:44 GMT on 13 (cf. Fig. 4) to 4:11 GMT on 14 (cf. Fig. 5). Polar low B then decays, beyond the possibility of tracking via its cloud fields. During the 15-h period of co-rotation, the vortices are separated by an average distance (d) of about 400 km, the same scale as the individual lows themselves (cf. Figs. 4 and 5).

Following the decay of first low B, and then low A, two more mesoscale polar lows C* and E develop in the same area; Fig. 7 shows an IR image at 5:39 GMT on 15 December 1982. The developments of C* and E are primarily convective in nature (RPPT). Low C* grows in scale from an "arctic instability low" (around 100 km in scale) to a mesoscale polar low (around 200 km in scale) by 15:00 GMT on 15 December 1982 (Fig. 8). Note two other arctic instability lows, C and D, (Fig. 2; Rasmussen, 1985a; RPPT) briefly

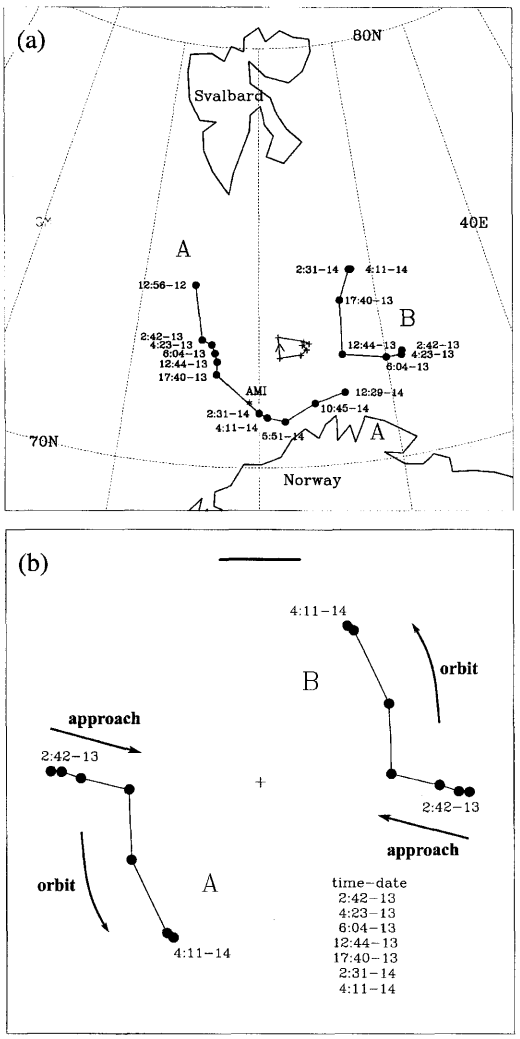

Fig. 6. (a) Tracks of polar lows A and B in the Barents Sea area. The time-dates of each satellite derived location are shown. The +'s indicate the centroid of the two polar lows. An asterisk marks the location of weather ship AMI. Note low A is longer lived than low B. (b) Centroid relative tracks of polar lows A and B, for the period of their co-existence. The time-dates of each location are tabulated. A scale is indicated by the horizontal bar, which has length 100 km.

develop, and then decay before C* and E. However they are considerably smaller in scale than the polar lows and so are not discussed further. Figs. 7, 8 show satellite imagery of polar lows C* and E at the beginning and end of their period of co-existence, at 05:39 GMT and 14:00 GMT on 15 December 1982. Again convective activity is indicated by the small cells of high cloud that are visible in the vortex circulations. The tracks of C* and E are plotted in Fig. 9a. Both lows track in a north to northwesterly direction, as does their centroid. The binary system is undergoing a mean translation at about 10 m s^{-1} as mapped out by the path of the centroid. Low C* lives longer than low E, which decays after about a 10 hour lifetime, on the ice around Svalbard. Fig. 9b plots the centroid relative motion of C* and E, and indicates a continuous cyclonic co-rotation, with perhaps an escape at the end of the period. Low E moves further during the period of their co-existence, because its northwesterly progression is enhanced by the binary interaction. Whereas low C* moves less far, as its motion is retarded by the binary interaction. An examination of the European Meteorological Bulletin mean-sea-level pressure charts (not shown) for this period shows a small trough stretching NE from a synoptic scale low. The trough covers the Barents Sea area — where the mesoscale lows C* and E appear in the imagery; the larger low system is centred to the SW of the binary pair at 3°W, 64°N at 00GMT and 4°E, 64°N at 12GMT on the 15th. This configuration is consistent with the translation of the binary system in a northwesterly direction by the larger scale low. Strong evidence that the low tracks of C* and E can be explained by a superposition of a co-rotation and a translation of the pair.

3.2. *Rotation rates*

The observed rotation rates of A and B, and C* and E are plotted in Figs. 10a, b respectively. The rotation rates of A and B show a marked increase from 0°–1° per hour during the approach phase to 2°— 6° per hour during the orbit phase. The error bars are calculated by assuming a small error (±0.05° of latitude which is 5.56 km) in the location of the centre of each low, which leads to an error bound on the rotation rate (ω) between 2 images (see the Appendix for details). Note that for relatively short time periods, there will be relatively large error bars, but a greater number of data points. Whereas for longer time periods, the error bars will be relatively small, but there will be fewer data points. Fig. 10b shows the

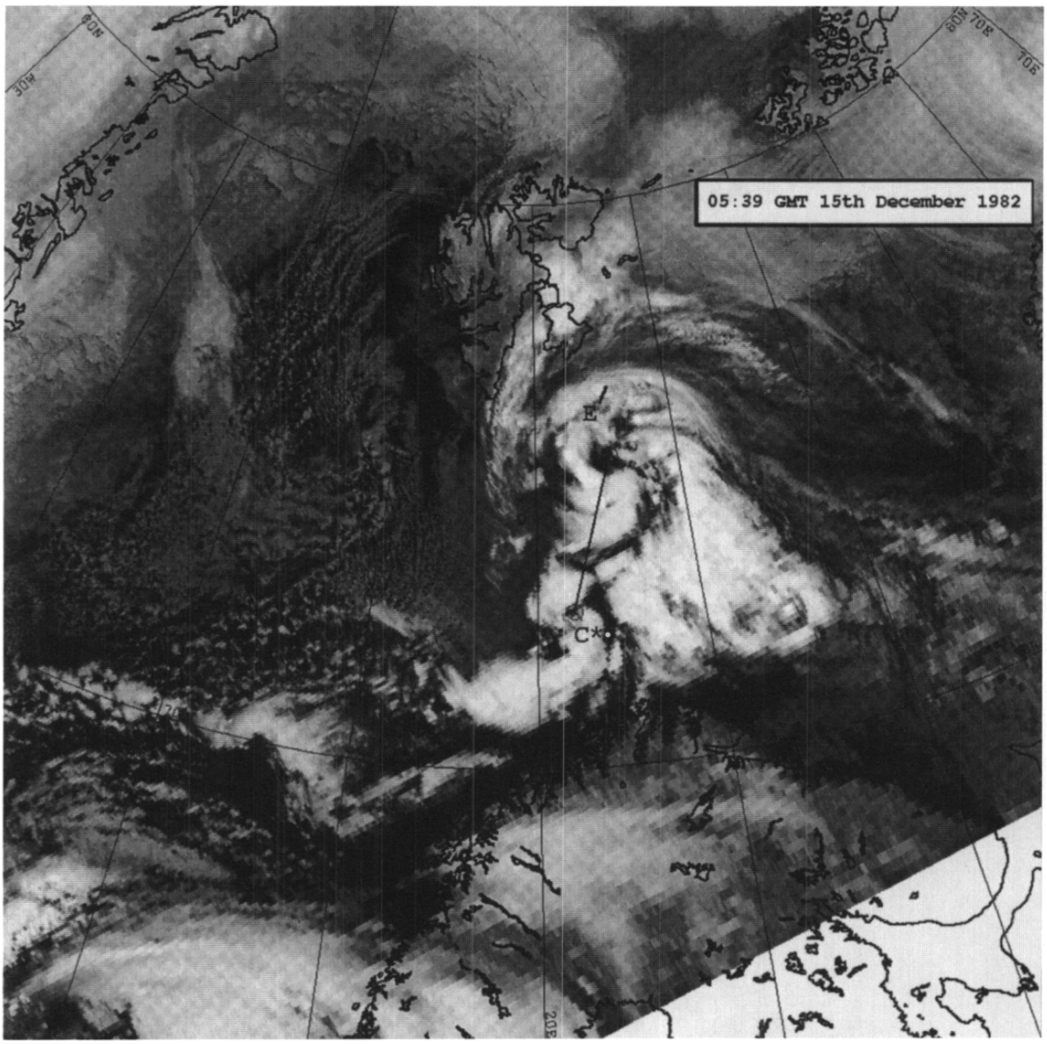

Fig. 7. IR satellite image at 05:39 GMT on 15 December 1982 from the NOAA-7 pass. Polar lows C* and E are marked. Note this image is at a lower resolution, 4 km pixels compared to the other images which are 1 km pixels.

observed rotation rates for C* and E over their period of co-rotation; in this case the rotation rates vary between approximately 2° and 8°/h.

Theoretical estimates of the rotation rates for the two pairs are also shown in Figs. 10a, b. The estimates are from the simple barotropic theory of eq. (3), so require estimates of V_m, R_m, and d. Polar low A passed over the weather ship AMI (marked on Fig. 6a), and a surface wind profile is available (Fig. 11a). This profile is broadly comparable to the axisymmetric Rankine vortex wind profile employed in the derivation of eq. (3): a linear wind increase from the vortex centre to a radius R_{Am}, with a $1/r$ wind profile outside this radius. The time-wind profile in Fig. 11a can be converted into a distance-wind profile by using an estimate of the translation speed of vortex A over the weather ship AMI. Between 17:40 GMT on the 13th and 2:31 GMT on the 14th the translation speed was 4.8 m s^{-1} (Fig. 6a). Hence, 6 h between 22:00 GMT and 4:00 GMT on Fig 11a (as low A moves over ship AMI) are

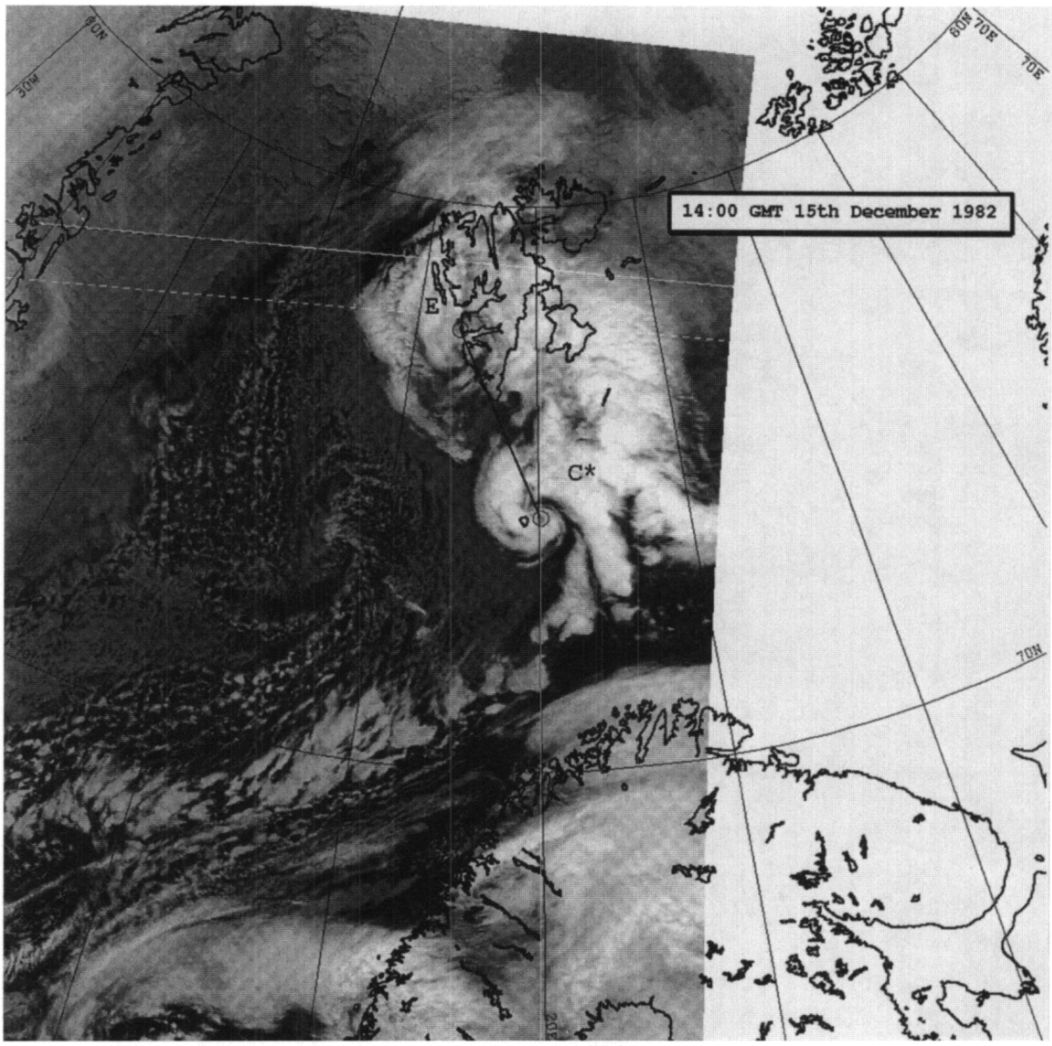

Fig. 8. IR satellite image at 14:01 GMT on 15 December 1982 from the NOAA-7 pass. Polar lows C* and E are marked.

equivalent to a distance of 104 km. The radius of maximum wind is therefore in the range $R_A =$ 25–35 km, with $V_{Am} =$ 23 m s^{-1} (Fig. 11a), and $d =$ 324–440 km over the orbit phase (Fig. 6b). Unfortunately we have no surface wind data for polar low B, however the satellite imagery (Figs. 4, 5) indicates that at this time low B was approximately the same size as A, so the same ranges for R_{Bm} and V_{Bm} are used. Maximum and minimum theoretical estimates of the rotation rates valid from 22:00 GMT on the 13th to 04:11GMT on the 14th (the end of the co-rotation period) are shown by the horizontal bold lines in Fig. 10a. The theoretical bounds for A and B have an excellent correspondence with the observed rotation rates.

A surface wind profile for vortex C*, taken as the low passed over the Bear Island weather station is shown in Fig 11b. As before this time-wind profile can be converted to a distance-wind profile using a translation speed of 10.8 m s^{-1}, calculated from the track of C* (Fig. 9b). So the

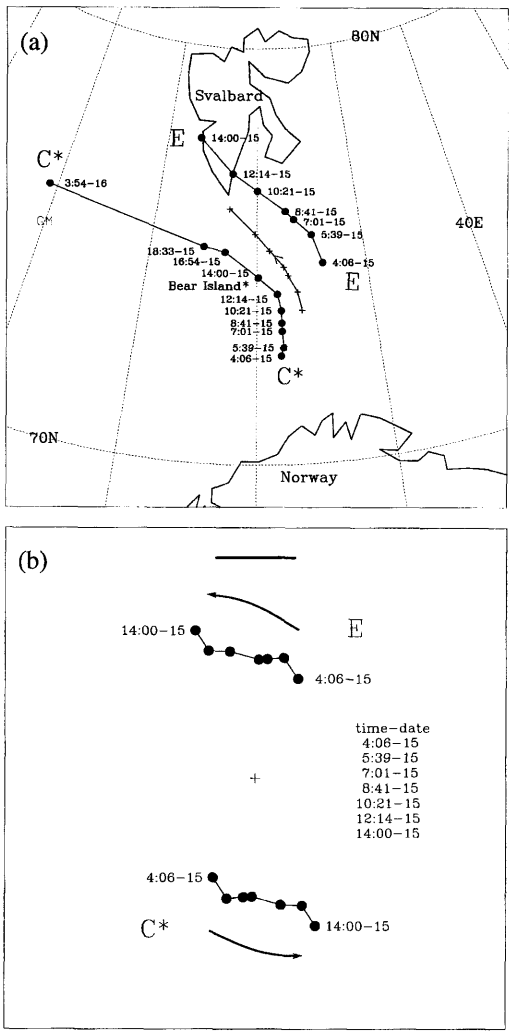

Fig. 9. (a) Tracks of polar lows C* and E in the Barents Sea area. The time-dates of each satellite derived location are shown and the +'s indicate the centroid of the two polar lows. An asterisk marks the location of the Bear Island meteorological station. Note low C* is longer lived than low E, but during their period of co-existence low E is moving faster. (b) Centroid relative tracks of polar lows C* and E, for the period of their co-existence. The time-dates of each location are tabulated. A scale is indicated by the horizontal bar, which has length 100 km.

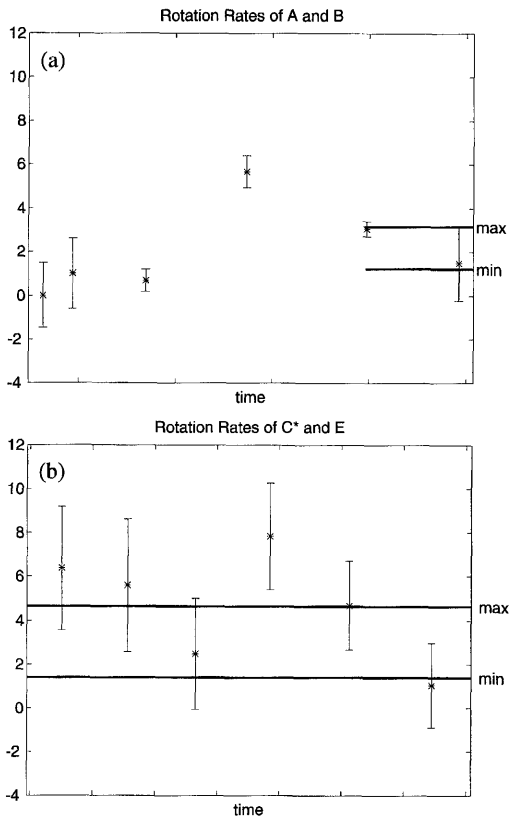

Fig. 10. Rotation rates over the periods of co-existence for polar lows (a) A and B, and (b) C* and E. The points show the observed rotation rates with error bars, and the bold horizontal lines show the maximum and minimum theoretical rotation rates calculated using eq. (3). The tick marks on the time axis are every 5.5 h for (a) and every 1.4 h for (b).

6 h from 12:00 GMT to 18:00 GMT on the 15 are equivalent to a distance of approximately 233 km. In addition, satellite derived wind speeds at 00:13 GMT on the 15th (Fig. 14 in RPPT) show maximum magnitudes of 16–18 m s^{-1} generated by vortices C* and E. These satellite derived surface winds and the satellite imagery available (Figs. 7 and 8) indicate that C* and E are comparable in size; with $R_{C*m} = R_{Em} = 40$–45 km, $V_{C*m} = V_{Em} = 15.5$–18 m s^{-1} (Fig. 11b) and $d = 268$–400 km (Fig. 9b). Substituting these into (3) gives the maximum and minimum theoretical bounds shown as bold lines in Fig. 10b. As the wind data brackets the full period of co-rotation, these bounds are taken to be valid for this whole period. Given the error bars, there is a good correspondence between the theoretical rotation rates and the observed rates; all but one of the observed rates lies within the bounds given by theory.

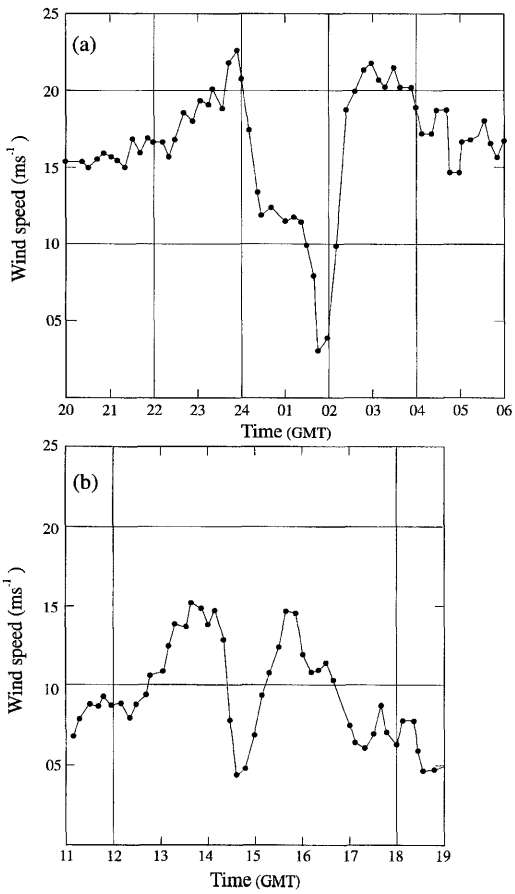

Fig. 11. Surface wind profiles for (a) polar low A as it passed over weather ship AMI from 22:00 GMT on 13th to 06:00 GMT on 14th December 1982; and (b) polar low C* as it passed over the Bear Island weather station from 11:00 to 19:00 GMT on 15th December 1982. The wind speeds are 10 minute means (after RPPT Figs. 12, 17).

3.3. Discussion

The observed movements of polar lows A and B, and C* and E, (Figs. 6a, 9a) are consistent with the binary interaction model. The polar low tracks are a superposition of a co-rotation around the centroid of the binary pair, and a translation of the binary pair by the ambient flow. In the case of lows A and B, there is little translation of the pair. The interaction fits into the Lander and Holland (1993) paradigm of approach, capture and orbit, before the decay of B. In the case of lows C* and E there is a steady northwesterly translation of the binary pair, indicating advection by a synoptic scale low to the southwest of the pair. The binary interaction between C* and E consists of an orbit phase, and then the decay of low E.

Overall there is a good correspondence between the observed rotation rates and estimates of these rates from the simple barotropic theory. The variations in the observed rotation rates over time may be due to several factors. In the case of A and B they mainly reflect the stages of the binary interaction. In the case of C* and E, small changes in the alignment of the vortex pair in the mean flow, or changes in the vortex structure may explain the variations of the observed rotation rates over the period. The difference between the theoretical estimates and the observed rotation rates will be due to several factors: for example the vortices are only approximately axisymmetric and Rankine, and their structure will undoubtedly change through time. If a stronger azimuthal wind profile is assumed (e.g., rather than $1/r$, a $1/r^a$ profile, for $a<1$) then systematically larger rotation rates would be estimated by the barotropic theory. The approximation of these convective systems by barotropic vortices will also lead to some degree of error.

It should be noted that the rotation rates for the binary pairs are independent of the position of the centroid of the pair, assuming that the ratio of the vortex "masses" remains fixed through the rotation period. This is discussed further in the Appendix. This means that our assumptions about the equality of vortices A and B, and C* and E, do not affect the observed rotation rates shown in Fig. 10. Although of course the chosen ranges for R_m, V_m, and d do affect the estimated rotation rates. The assumption of equality only affects the estimated path of the centroid, as plotted in Figs. 6b, 9b for example. A comparison of the path of the centroid with the relevant synoptic charts can provide a check on whether the translation of the binary system is consistent with the environmental flow. As noted above, if C* and E are assumed equal in mass, the centroid has a path which is consistent with the northwesterly translation of the system by a synoptic scale low to the southwest.

4. The March 1992 case

The 2nd polar low episode discussed here occurred in March 1992 in the Norwegian and

Barents Seas. This period was suggested by the study of Ørbæk and Naustvik (1995, hereafter ØN) where several convective disturbances were shown to exist during a 4-day period. Their study registered infrasonic signatures of the disturbances using two passive broadband infrasonic sodars. These instruments can "hear" convective activity as it is a strong acoustic generator. Although an interesting idea, unfortunately there are serious limitations to the technique. Strong local winds can shield the infrasonic detector from the disturbances of interest, and also no indication of the amplitude of the acoustic generator is given; only an active/nonactive convective signal is produced. The ØN study demonstrated the existence of several convective disturbances in the sodar measurements, and this was corroborated by cloud patches observed in the satellite imagery. However an independent examination of AVHRR satellite imagery from 23 to 26 March 1992 was disappointingly bereft of well defined cloud circulations. The main arctic low focussed upon in ØN (their number 1) had a well defined comma-shaped cloud signature, but the other co-existing disturbances were either an order of magnitude smaller (around 50 km in scale) or had rather amorphous cloud signatures. The case was not as fruitful in terms of vortex interactions as had been hoped. In fact the tracks of disturbances 2 and 3 (in Fig. 2 of ØN) were found to be a number of consecutive atmospheric cloud features or small scale arctic instability lows growing on frontal zones, rather than coherent vortices lasting for several days as implied by their study.

Towards the end of the period on 27th March 1992, two atmospheric vortices did co-exist and interact for approximately 12 h. Fig. 12 shows lows U and V in the Barents Sea area at 08:35 GMT on 27 March 1992. Low U is centred in a mesoscale (1000 km scale) low system with a well defined spiral cloud signature consisting mainly of convective cells. It appeared to be the case that low U was an example of a "cold-low" type of system (Businger and Reed, 1989), i.e., low U is coherent within the shell of an older larger scale low. Examination of the previous 24 h of images showed the 1000 km mesoscale low dominated the Barents Sea area for around a day. It was characterised by high cirrus cloud bands with some convection in its centre. Imagery 4 h earlier and 4 and 6 h later (not shown) indicate low V increasing in magnitude, and becoming more convectively active over this period.

The tracks of U and V are plotted in Fig. 13a, in part (a) in geographic coordinates, and in part (b) in centroid relative coordinates. The locations are taken from all the high quality imagery available. A cyclonic co-rotation is evident over the 10-h period, and there is a small easterly translation of the binary system as illustrated by the path of the centroid in Fig. 13a. The rotation rates for the three time intervals are 5.62°/h (from 3:57 to 8:35 GMT), 3.90°/h (from 8:35 to 12:11 GMT) and 2.74°/h (from 12:11 to 13:51 GMT). No theoretical estimates of the rotation rates are calculated as high temporal resolution surface wind profiles were not available. However 3 hourly surface wind observations for the Bear Island station (74.5°N, 19.0°E) were available, these record a backing of the wind from a 7.7 m s^{-1} southeasterly at 00 GMT, to 5.1 m s^{-1} easterly at 03 GMT, to 7.7 m s^{-1} northeasterly at 06 GMT, to between a 10.3–12.9 m s^{-1} north-northeasterly from 09 to 21 GMT on 27 March 1992. This backing is consistent with the station being influenced by the outer circulations of firstly low U and then low V over the day, in other words also consistent with the tracks plotted in Fig. 13a.

Overlaid on Fig. 12 are contours of surface wind speed derived from the Special Sensor Microwave/Imager (SSM/I), see Claud et al. (1992) and Moore et al. (1996) for further details. Only a surface wind *speed* is available from this instrument, which means there are ambiguities in interpreting the data in terms of a vector wind field. In Fig. 12, U lies with a maximum in wind speed to the west of the cloud vortex centre, a minimum in wind speed between U and V, and increases in wind speed towards the centre of V. The minimum between U and V can be explained by the summation of southerlies induced by low U and northerlies induced by low V cancelling each other to give low wind speeds. This cancellation would not occur on the "outsides" of vortices U and V, i.e., to the west of U and the east of V, where there are indeed higher wind speeds. Other data times for the 27 March 1992 were examined and these showed generally similar patterns.

In summary, the evidence suggests that the binary interaction model may apply to lows U and V in this second polar low episode, but a

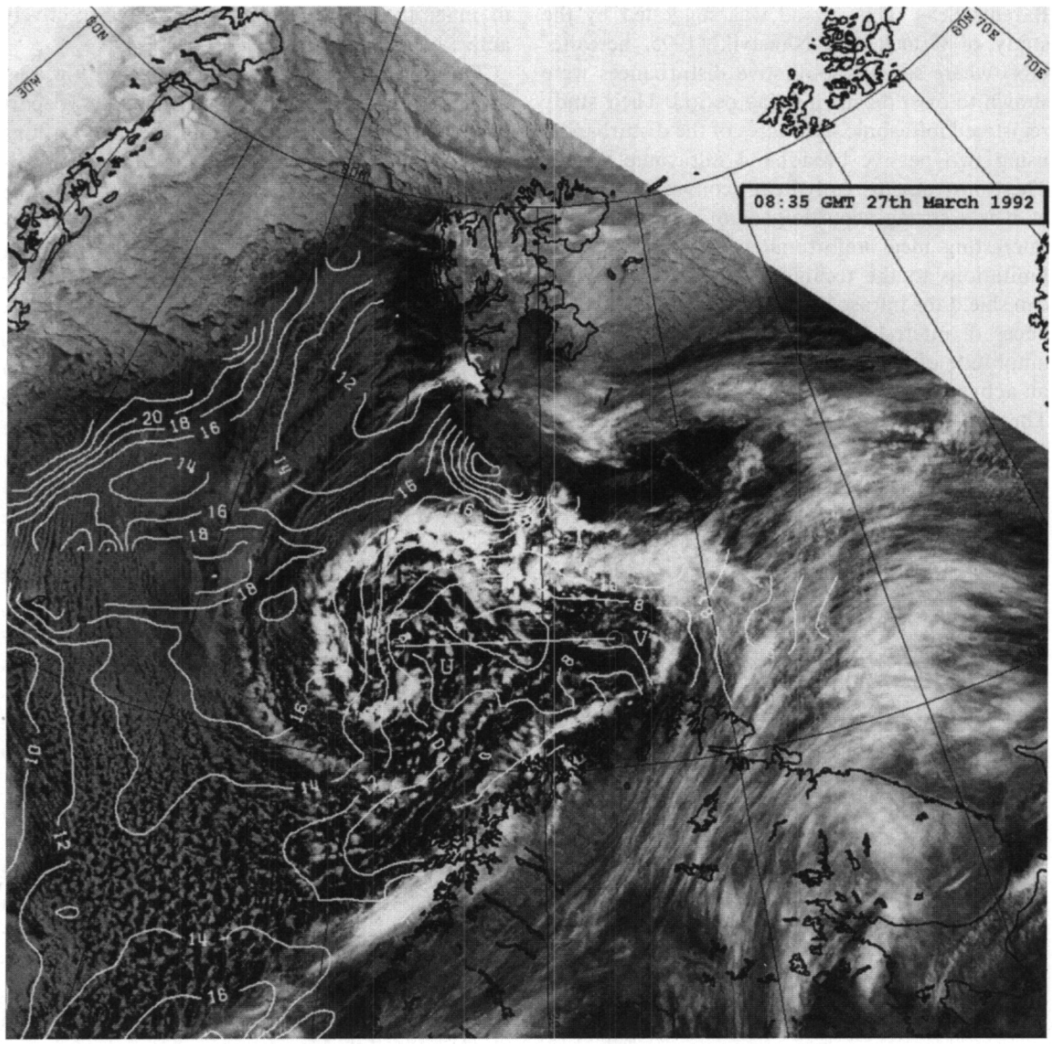

Fig. 12. IR satellite image of the Barents Sea area, at 08:35 GMT on 27 March 1992 from the NOAA-12 pass. Polar lows U and V are marked. Contours of surface wind speed (every 2 m s^{-1}) as derived from the SSM/I F11 pass at 06:32 GMT on 27 March 1992 are overlaid. It is interesting to note the vortex street to the south of Jan Mayen Island at 71°N, 8°W.

quantitative confirmation, carried out by comparing rotation rates, was unfortunately not possible.

5. Conclusions

When two polar lows are in the same area, binary interactions may occur that are similar to the vortex motions first noted by Fujiwhara (1923, 1931). These binary interactions consist primarily of a cyclonic co-rotation of the polar lows around their centroid, induced by mutual advection. In addition, the whole binary system may be advected by the surrounding environmental flow. Hence the polar lows' movements consist of a superposition of a cyclonic co-rotation and a translation of the binary system. The co-rotation is clear in centroid relative coordinates; the translation is clear from the path of the centroid in geographic coordinates.

A simple barotropic model is detailed, following

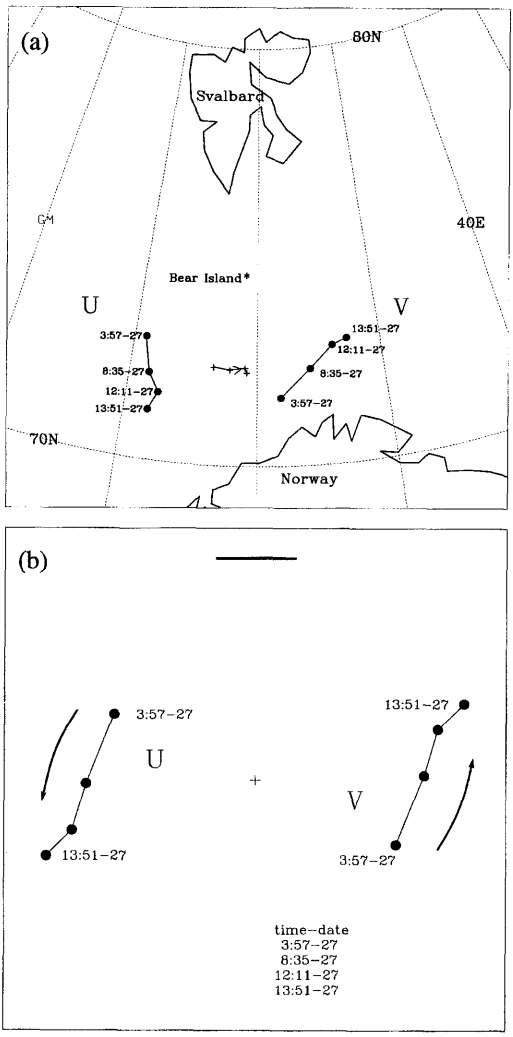

Fig. 13. (a) Tracks of polar lows U and V in the Barents Sea area. The time-dates of each satellite derived location are shown. The +'s indicate the centroid of the two polar lows. An asterisk marks the location of the Bear Island meteorological station. (b) Centroid relative tracks of polar lows U and V, for the period of their co-existence. The time-dates of each location are tabulated. A scale is indicated by the horizontal bar, which has length 100 km.

Haurwitz (1951), assuming each vortex is a Rankine vortex. This allows a theoretical estimate of the rotation rates of the polar lows from certain properties of each low, in this case surface wind profiles of each low. There is a good correspondence between the observed rotation rates and theoretical estimates of the rotation rates, indicating the binary interaction model can explain the majority of the cyclones' motion.

In the cases studied here the binary interaction occurs in the later, convective stage of development, when the polar lows are somewhat analogous to arctic hurricanes (Emanuel and Rotunno, 1989). Furthermore, a similar co-rotation phenomenon has been well documented amongst tropical cyclones and so the discovery of binary interactions between polar lows provides another link between polar lows and tropical cyclones. Indeed it can be argued that such interactions would be expected at low latitudes, where the vortices are strong compared to the ambient flow; and at high latitudes, where the vortices are intense yet small compared to the scale of the varying mean flow; in contrast to mid-latitudes, where synoptic lows are on the same scale as the mean flow, and where the zonal mean flow is strongest.

It is worth noting that the periods of co-rotation documented here for binary polar lows represent a substantial part of the polar low lifetimes. Although the periods of co-rotation are relatively short: 15, 10 and 10 h, for lows A and B, C* and E, and U and V, respectively. This is a substantial part of their lifetimes, which ranged from approximately 10 h (E and V) to 48 h (A) in this study. At low latitudes, tropical cyclones can take days to spin up, and have lifetimes of 3–15 days. Binary interactions can last from 3 to 6 days (Lander and Holland, 1993), therefore represent a similar proportion of the life-cycle of tropical cyclones, as the co-rotations documented here do for polar low life-cycles. One can think of the "metabolism" of weather systems at high latitudes as being very high. For example the large Coriolis parameter, and shallow troposphere lead to short e-folding times, small horizontal scales and fast life-cycles for instabilities (Reed and Duncan, 1987; Craig and Cho, 1988). In contrast to low latitudes, where the "metabolism" of large scale weather systems is low, for the opposite reasons, a small Coriolis parameter and a deep troposphere.

When two or more polar lows exist in the same area, binary interactions should be an important consideration in forecasting the tracks of the polar lows, since the co-rotation would drastically alter the path and translation speed of each vortex. For example, in Fig. 6a polar low A moves from a

southerly direction to an easterly direction during its interaction with B, thus encountering the coast of Norway considerably further north and east of the point where a non-interacting track would have taken it. In theory such interactions should be captured by the dynamics of operational forecast models. Unfortunately however, capturing polar lows, and modelling realistically their structure is at the limit of current forecast models. In discussions with forecasters during this study, the impression was that operational models still have difficulty predicting polar low development and so will also have difficulty predicting an interaction process. In the time-being, a manageable alternative would be monitoring satellite imagery for binary polar low occurrences, whereupon upon suitable adjustments could be made to the forecast tracks of the polar lows.

6. Acknowledgements

The authors would like to thank Erik Rasmussen for the use of rare satellite imagery of the December 1982 case, and also John Turner and Bob Crawford for assistance with other data sources. All the satellite imagery shown was from the NERC Satellite Station at the University of Dundee, UK, (except Fig. 7 which was from the NOAA National Climatic Data Center, North Carolina, USA) and was processed with the Terascan software package. The data support section at NCAR provided the Bear Island station data for the March 1992 case. Khader Khan at the University of Toronto helped with redrawing Fig. 11. We would also like to thank Keith Alverson and George Craig for useful discussions on this work, as well as the members of the European Polar Lows Working Group for their helpful comments. Funding for this study was provided by Environment Canada and the Office of Naval Research.

7. Appendix

Error analysis

There are several sources of error in estimating the location and rotation rates of the observed polar lows. There is a geolocation error in processing the satellite data due to discrepancies in the perceived versus actual orbital elements of the pass, and also due to small pitching and yawing movements of the satellite itself. This error can be estimated from a comparison of actual coastlines with the overlaid coastlines generated in the Terascan software package. A number of images were examined and the geolocation errors were in the range 3–7 km, with no preferential direction in the error. Errors in time are negligible as the pass time is known to the nearest minute. So the other main concern is determining the centroid (the "centre-of-mass") of the system. If we assume that the properties of the two lows are in a constant ratio over the time of co-rotation (eq. (4) is constant over time), then the rotation rate is independent of this ratio. This can be understood from geometric arguments by noting that the centroid is always located on the connection line joining the centre of the lows. This means that the observed rotation rates in Fig. 10 are independent of the relative magnitudes of the two vortices. Hence one possible source of error is eliminated, and the conclusion that binary interactions can explain the observed cyclone motion is strengthened.

The path the centroid maps out is the movement of the entire binary system, and so indicates advection of the system by the environmental flow. Hence it is possible to compare the centroid's path with the environmental flow, as a check on the dynamics of the binary interaction model. This was done for the December 1982 case for lows C* and E; in this case the path of the centroid was in a north to northwesterly direction which fitted the synoptic situation of a depression to the southwest over northern Scotland.

Thus the major source of error in rotation rate calculation is a location error: due to the geolocation error, and due to the subjective nature of locating the centre of circulation from the cloud fields. This subjective error is rather difficult to quantify, although fortunately in many cases a clear central eye identifies the low centre and the eye is coherent in time. The results of an error analysis for the binary system co-rotation are shown in Fig. 14. This plots error in rotation rate (in degrees per hour) versus location error, for a fixed distance between the lows of $d = 400$ km. The error is a function of $sin^{-1}(2a/d)$, where a is the location error. The function sin^{-1} is close to linear for small arguments, so the curves in Fig. 14 are

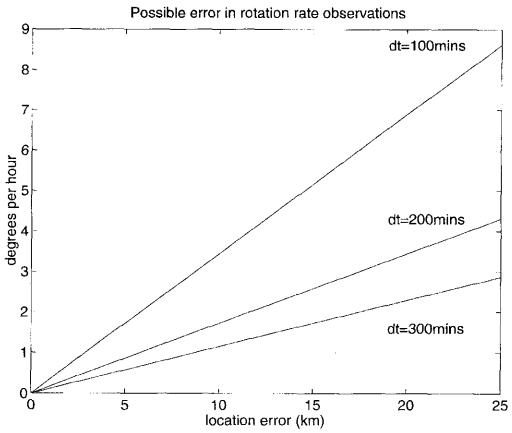

Fig. 14. Possible error in observed rotation rates as a function of location error. Three curves are plotted for time intervals equal to 100, 200 and 300 minutes (note there are approximately 100 minutes between adjacent polar orbiting satellite passes).

close to linear. Hence the error in rotation rate is approximately proportional to the error in location, for small errors in location. A notional location error of $\pm 0.05°$ latitude (5.56 km), indicated by the error bars in Fig. 10, is chosen to give a representative error in rotation rate. This value was chosen as a reasonable estimate of the combined location errors discussed above. It should be noted that as rotation *rates* are plotted $(d\omega/dt)$: for relatively short time periods there will be relatively large error bars. Whereas for longer time periods the error bars will be smaller, but there will be fewer data points. There is a trade off between frequency of data and the size of the possible errors in rotation rate. This is illustrated in Fig. 10 where in (a) the data are spaced every few hours with relatively small error bars, and in (b) the data are every satellite pass (100 mins), and the error bars are consequently relatively large. We have confidence in both results as in (a) the error bars are small, and in (b) most of the data points (and their mean) lie between the maximum and minimum thresholds.

REFERENCES

Anthes, R. A. 1982. Tropical cyclones. Their evolution, structure and effects. *Am. Meteor. Soc.* 208.

Batchelor, G. K. 1980. *An introduction to fluid mechanics.* Cambridge University Press, Cambridge, UK.

Businger, S. and Reed, R. J. 1989. Polar lows. In: *Polar and arctic lows*, eds. Twitchell, P. F., Rasmussen, E. A. and Davidson, K. L. Deepack Publishing, Virginia, USA.

Brand, S. 1970. Interaction of binary tropical cyclones of the western North Pacific Ocean. *J. Appl. Meteor.* **9**, 433–441.

Claud, C., Katsaros, K. B., Petty, G. W., Chedin, A. and Scott, N. A. 1992. A cold air outbreak over the Norwegian Sea observed with the TIROS-N Operational Vertical Sounder (TOVS) and the Special Sensor Microwave/Imager (SSM/I). *Tellus* **44A**, 100–118.

Craig, G. C. and Cho, H. -R. 1988. Cumulus heating and CISK in the extratropical atmosphere. Part I: Polar lows and comma clouds. *J. Atmos. Sci.* **45**, 2622–2640.

Craig, G. C. and Cho, H. -R. 1992. A study of two cases of comma-cloud cyclogenesis using a Semigeostrophic model. *Mon. Wea. Rev.* **120**, 2942–2961.

Dong, K. and Neumann, C. J. 1983. On the relative motion of binary tropical cyclones. *Mon. Wea. Rev.* **111**, 945–953.

Emanuel, K. A. and Rotunno, R. 1989. Polar lows as arctic hurricanes. *Tellus* **41A**, 1–17.

Fuijwhara, S. 1923. On the growth and decay of vortical systems. *Quart. J. Roy. Meteor. Soc.* **49**, 287–293.

Fuijwhara, S. 1931. Short note on the behaviour of two vortices. *Proc. Phys. Math. Soc. Japan Ser 3.* **13**, 106–110.

Gill, A. E. 1982. *Atmosphere-ocean dynamics.* Academic Press, London, UK.

Haurwitz, B. 1951. The motion of binary cyclones. *Arch. Meteor. Geophys. Bioklim.* **B4**, 73–86.

Holland, G. J. and Lander, M. 1993. The meandering nature of tropical cyclone tracks. *J. Atmos. Sci.* **50**, 1254–1266.

Holland, G. J. and Dietachmayer, G. S. 1993. On the interaction of tropical-cyclone-scale vortices (III). Continuous barotropic vortices. *Quart. J. Roy. Meteor. Soc.* **119**, 1381–1398.

Hopfinger, E. J. and van Heijst, G. J. F. 1993. Vortices in rotating fluids. *Ann. Rev. Fluid Mech.* **25**, 241–289.

Hoskins, B. J., McIntyre, M. E., and Robertson, A. W. 1985. On the use and significance of isentropic potential vorticity maps. *Quart. J. Roy. Meteor. Soc.* **111**, 877–946.

James, I. N. 1994. *Introduction to circulating atmospheres.* Cambridge University Press, Cambridge, UK, 444pp.

Lander, M. and Holland, G. J. 1993. On the interaction of tropical-cyclone-scale vortices (I). Observations. *Quart. J. Roy. Meteor. Soc.* **119**, 1347–1361.

Midtbø, K. H. 1986. Polar low forecasting. In: *Proc., The International Conference on Polar lows.* The Norwegian Meteorological Institute.

Moore, G. W. K., Reader, M. C., York, J. and Sathiya-

moorthy, S. 1996. Polar lows in the Labrador Sea. A case study. *Tellus* **48A**, 17–40.

Ørbæk, J. B. and Naustvik, M. 1995. Infrasonic signatures of a polar low in the Norwegian and Barents Sea on 23–27 March 1992. *Tellus* **47A**, 921–940.

Rasmussen, E. A. 1985a. A case study of a polar low development over the Barents Sea. *Tellus* **37A**, 407–418.

Rasmussen, E. A. 1985b. A polar low development over the Barents Sea. *Technical report no. 7 of the polar lows project*, available from DNMI.

Rasmussen, E. A. 1989. A comparative study of tropical cyclones and polar lows. In: *Polar and arctic lows*, eds. Twitchell, P. F., Rasmussen, E. A. and Davidson, K. L. Deepack Publishing, Virginia, USA.

Rasmussen, E. A., Pedersen, T. S., Pedersen, L. T. and Turner, J. 1992. Polar lows and arctic instability lows in the Bear Island region. *Tellus* **44A**, 133–154.

Reed, R. J. and Duncan, C. N. 1987. Baroclinic instability as a mechanism for the serial development of polar lows. A case study. *Tellus* **39A**, 376–384.

Ritchie, E. A. and Holland, G. J. 1993. On the interaction of tropical-cyclone-scale vortices. II: Discrete vortex patches. *Quart. J. Roy. Meteor. Soc.* **119**, 1363–1379.

Vautard, R. 1990. Multiple weather regimes over the North Atlantic: Analysis of precursors and successors. *Mon. Wea. Rev.* **118**, 2056–2081.

Wang, Y. and Holland, G. J. 1995. On the interaction of tropical-cyclone-scale vortices. IV: Baroclinic vortices. *Quart. J. Roy. Meteor. Soc.* **121**, 95–126.

Ziv, B. and Alpert, P. 1995. Rotation of binary cyclones — a data analysis study. *J. Atmos. Sci.* **52**, 1357–1369.